CAR T cell engineering impacts antigen-independent activation and co-inhibition

Simon Stücheli[1,2*], Christoph Schultheiß[1,2*], Paul Schmidt-Barbo[1,2], Andreas Zingg[1,3], Natascha Franz[1,2], Sarah Adamo[4,5], Claudia Fischer[1,2], Heinz Läubli[1,3], Mascha Binder[1,2]

[1] Division of Medical Oncology, University Hospital Basel, Basel, Switzerland,

[2] Laboratory of Translational Immuno-Oncology, Department of Biomedicine, University and University Hospital Basel, Basel, Switzerland,

[3] Laboratory of Cancer Immunotherapy, Department of Biomedicine, University and University Hospital Basel, Basel, Switzerland,

[4] Department of Medicine Huddinge, Center for Infectious Medicine, Karolinska Institutet, Stockholm 14152, Sweden,

[5] Department of Biomedicine, University and University Hospital Basel, Basel, Switzerland.

[*] These authors contributed equally: SS, CS

Correspondence to:
Mascha Binder, MD, Division of Medical Oncology, University Hospital Basel, Petersgraben 4, 4031 Basel, Switzerland
Phone (+) 41 79 416 5839
E-mail: Mascha.Binder@usb.ch

Abstract

Viral vectors have successfully modified T cells to express chimeric antigen receptors (CAR), leading to clinical approvals. However, their high cost and regulatory challenges hinder rapid and broad clinical translation. Here, we demonstrate that our lentivirally (LV) manufactured R110-CAR T cells, targeting a leukemia neoepitope, can also be engineered using non-viral Sleeping Beauty (SB) transposition with minimal-sized DNA vectors. Flow cytometry and single-cell sequencing was used to compare the two production modes using healthy donor and CLL patient-derived T cells and a CD19-CAR T cell control. SB products were shifted towards $CD8^+$ subsets with expression of activation/co-inhibition markers (CD69, LAG-3, TIM-3) despite their naïve-like phenotype and lack of antigenic challenge. The CAR binding moiety modulated these patterns with R110-CAR T cells showing more aberrant phenotypes. Moreover, SB engineering resulted in inflammatory signatures along with RIG-I-like and TOLL-like nucleotide sensing potentially resulting from the transfection procedure. Patient-derived products showed significantly fewer CAR-expressing cells, reduced proliferation clusters, and lower T cell diversity, particularly with SB manufacturing, pointing at potential challenges with this method when engineering CLL T cells. Together, our data suggest that the engineering mode may substantially influence T cell properties and that these are further modulated by the CAR binding moiety and the type of T cell donor.

Introduction

Chimeric antigen receptor (CAR) T cells are powerful tools in oncology, offering a promising approach for targeted cancer therapy (1, 2). However, beyond the availability of tumor-specific target molecules, logistical complexity and high costs of manufacturing of autologous viral products limit CAR T cell availability (3, 4). Other manufacturing procedures such as sleeping beauty (SB) transposition of CAR genes may overcome some of these – especially financial – limitations, but such products are still experimental and no commercial SB-manufactured product has been licenced so far (5, 6).

Comparative studies on CAR T cell properties according to the mode of production are scarce, especially regarding their activation and co-inhibition profile. In the context of autologous CAR T cell therapy, where a patient's own often dysfunctional T cells are harvested, engineered, and reinfused, T cell inhibition is particularly problematic (7). When these T cells are further subjected to the stress of genetic modification and expansion, their efficacy can be further diminished. This is exemplified by CAR T cells from healthy donors being better at controling tumor growth in an in vivo model compared to CAR T cells derived from chronic lymphocytic leukemia (CLL) patients (8). Moreover, certain single-chain variable fragments (scFvs) are associated with ligand-independent tonic signalling, which has been shown to reduce the efficacy of CAR T cells, thereby limiting their therapeutic potential (9-11). This includes diminished cytokine production, reduced proliferative capacity, and impaired cytotoxic activity accompanied by the upregulation of inhibitory receptors such as PD-1, TIM-3, and LAG-3 (9, 12). Whether the CAR-inherent level of tonic signaling may be modulated by the production mode remains unclear at this point.

In the work presented here, we show that our previously published lentivirally (LV) manufactured CAR T cells that are directed against the CLL neoepitope IGLV3-21^{R110} (named anti-R110) (13), can be engineered through non-viral SB transposition of CAR

genes. This production method resulted in about equal efficacy of transgene expression, but the pattern of T cell differentiation, activation and co-inhibition markers were substantially different and partially modulated by the specific CAR.

Materials and Methods

Cell lines and CLL patient and healthy donor blood cells

HEK293T, K562 and NALM-6 cells were purchased from the DSMZ (German Collection of Microorganisms and Cell Cultures GmbH). For ectopic expression of the IGLV3-21^{R110} light chain in NALM-6 cells (NALM-6-R110), the coding sequence was cloned into the Lentiviral Gene Ontology (LeGO) vector LeGO-iZeo2 and positively transfected cells were selected by culturing cells in the presence of 0.3 mg/mL zeocin (#ant-zn-1, InvivoGen, Toulouse, France). NALM-6 and NALM-6-R110 cells were maintained in RPMI-1640 (#61870, Thermo Fisher Scientific, Waltham, MA, USA), K562 in IMDM (#I3390, Sigma-Aldrich, St. Louis, MO, USA) and HEK293T in DMEM (#31966-021, Thermo Fisher Scientific) medium. All three media were supplemented with 10% heat-inactivated fetal bovine serum, 100 U/mL penicillin and 100 µg/mL streptomycin.

Blood samples from CLL patients were collected after informed consent as approved by the ethics committees of Halle-Wittenberg. Peripheral mononuclear cells (PBMCs) from CLL patients or healthy donors were isolated by Ficoll gradient centrifugation and primary T cells isolated using the Pan T Cell Isolation Kit (#130-096-535, Miltenyi Biotec, Bergisch Gladbach, Germany).

Lentiviral production

Five million HEK293T cells were seeded per 10 cm dish. After 24 hours, the medium was replaced with fresh medium containing 25 µM chloroquine. The cells were then transfected with the lentiviral vector containing the CAR sequence of interest along with lentiviral

packaging plasmids using the calcium phosphate transfection method (13). Five hours post-transfection, the medium was changed and the cells were incubated for three days. Subsequently, the supernatant was collected, filtered (0.2 µm), mixed with a 40% w/v PEG-8000 solution (25% PEG solution, 75% supernatant) and stored at 4°C overnight. The mixture was centrifuged (4°C, 45 minutes, 1500 rcf), the supernatant discarded, and the viral particles resuspended in activation medium (RPMI-1640, 10% heat-inactivated human serum, 100 U/mL penicillin, 100 µg/mL streptomycin, 50 µM 2-mercaptoethanol, 25 IU/mL IL-2 [#78036.1, StemCell Technologies, Vancouver, BC, Canada], 10 ng/mL IL-15 [#200-15-50UG, PeproTech, Thermo Fisher Scientific]). The viral particles were either immediately used for T cell transfection or stored at -80°C.

Preparation of CAR T cells by lentiviral transduction or sleeping beauty transposition

For lentiviral transduction, T cells were activated using CD3/CD28 Dynabeads (#11132D, Thermo-Fisher Scientific) in a 24-well format (1 × 10□ cells per well, bead-to-cell ratio 1:1) in activation medium. After 24 hours, 66% of the medium was replaced with fresh activation medium containing 0.5 mg/mL Synperonic-F108 and lentivirus encoding the respective CAR constructs. Following an additional 24 hours, 50% of the medium was replaced with fresh activation medium. After another 48 hours, the T cells were transferred to PRIME XV T-Cell CDM (91154-1L, FUJIFILM Irvine Scientific, Santa Ana, CA, USA) containing 10 ng/mL IL-15, and placed in a G-Rex-24-well format (#80192M, Wilson Wolf, St. Paul, MN, USA). On day 6 (144 hours post-T cell seeding), the CD3/CD28 beads were removed, and the medium was replaced.

For CAR T cell production using the SB transposase system, T cells were similarly activated using CD3/CD28 Dynabeads (bead-to-cell ratio 1:1) in activation medium. After 72 hours, 10 × 10□ T cells were electroporated using the MaxCyte GT Electroporation System (MaxCyte, Rockville, MD, USA) following its T Cell Protocol 3. The electroporation

was performed in the presence of 40 µg/mL SB transposase mRNA (custom-made by Etherna [Niel, Belgium] with CleanCap [TriLink, San Diego, CA, USA] and a plasmid-encoded polyA tail [94A]) and 150 µg/mL GenCircle CAR vector construct (GenScript, Piscataway, NJ, USA) in PRIME XV T-Cell CDM, using R-50x3 cuvettes (#ER050U3-10, MaxCyte). Electroporated T cells were immediately transferred to a G-Rex-24-well format, and after four hours, IL-15 was added to achieve a final concentration of 10 ng/mL. On day 6 (144 hours post-T cell seeding), the CD3/CD28 beads were removed.

All CAR T cells used in this study were generated from freshly isolated T cells and cultured at 37°C in a 5% CO_2 atmosphere in PRIME XV T-Cell CDM with 10 ng/mL IL-15. The medium was refreshed once per week.

In vitro coculture assays

Target cells seeded at 3×10^4 cells/well in a 96-well plate were co-incubated with effector cells at effector-to-target (E:T) ratio 5:1 or 1:1 in standard RPMI-1640 media (10% heat-inactivated fetale bovine serum, 100 U/mL penicillin, 100 µg/mL streptomycin). Only $scFv^+$ CAR T cells as determined by flow cytometry were considered effector cells. Immediately after combining target and effector cells, half of each well was subjected to flow cytometric analysis and the other half incubated for 24 hours.

Killing of target cells was assessed by gating for viable (DAPI-negative, #130-111-570, Miltenyi Biotec) $CD3^-$,$CD19^+$,$R110^+$ target NALM-6-R110 cells and by normalizing their percentage after 24 hour incubation to 0 hour incubation time. The same normalization was applied to DAPI-negative,$CD3^-$,$CD19^-$,$R110^-$ non-target K562 cells. Furthermore, the resulting values were used for an additional normalization step (Equation 1).

$$Equation\ 1\text{:}\ 1 - \left(\frac{\left[\frac{\%\ target\ at\ 24h}{\%\ target\ at\ 0h}\right]}{\left[\frac{\%\ non-target\ at\ 24h}{\%\ non-target\ at\ 0h}\right]} \right)$$

Flow cytometry was performed by washing the cells with PBS, followed by an incubation with primary unlabeled antibodies in staining buffer (1% w/v bovine serum albumin in PBS) for 30 min at 4°C in the dark. Cells were washed washed with PBS, incubated with labeled secondary antibodies and labeled primary antibodies in staining buffer for 30 min at 4°C in the dark, washed by PBS, resuspended in DAPI (1:200 dilution) and measured on a CytoFLEX S (Beckman Coulter, Brea, CA, USA). T-distributed stochastic neighbor embedding (tSNE (14)) analysis was performed by concatenating the duplicate measurements of the samples and using the embedded tSNE function of FlowJo (v10.10) with standard settings after gating for single $DAPI^{-}$,$CD3^{+}$ cells. Antibodies used for flow cytometry were diluted at 1:200 unless otherwise specified and listed in Supplementary Table 1.

Single-cell RNA and VDJ sequencing

Single-cell RNA and T cell receptor (TCR) VDJ sequencing was performed using the Chromium Next GEM Single Cell 5' Kit v2, Human TCR Amplification, and Human TCR Amplification kits (10X Genomics, Pleasanton, CA, United States) as described previously (15, 16). For library preparation, live (DAPI-negative) T cells from the SB and LV expansion cultures were FACS-sorted after staining the cells at 4°C for 30 min using a FITC-labeled anti-CD3 (clone SK7, #345763, BD BioSciences, Franklin Lakes, NJ, USA) antibody. Quality control steps were performed using an Agilent TapeStation (Agilent Technologies, Inc., Santa Clara, CA, United States). Sequencing was done on an Illumina NovaSeq 6000 system (Illumina, San Diego, CA, United States). Raw gene expression and TCR data were processed to read counts with the Cell Ranger pipeline (v7.0.1) (10X Genomics), which includes alignment to the human reference genome (GRch38), filtering and barcode counting. Processed read count matrices were analyzed and plotted using Seurat (v5.0.3) (17), scRepertoire (18) or scplotter package

(https://github.com/pwwang/scplotter) in RStudio (v2023.06.1; R version 4.3.1 (2023-06-16)). Integration of the single samples were performed using Harmony (19). To detect CAR T cell-specific sequences within the data, we created a custom reference genome based on the applied CAR T construct sequences using the cellranger mkref pipeline. Mean cluster expression per feature was calculated using Seurat's *AggregateExpression* function. Gene set scores were calculated and plotted using the UCell package (20). Heatmaps were generated using the pheatmap package. Differentially expressed genes (DEGs) were identified using Seurat's *FindMarkers* function (test.use = "wilcox", min.pct = 0.1, logfc.threshold = 0.1) and visualized using the EnhancedVolcano package. Gene set enrichment analyses (GSEA) were performed using the fgsea package (version 1.26.0). Human Hallmark category gene sets (e. g. KEGG, GO) were obtained from the Molecular Signatures Database (MSigDB) using the msigdbr R package. DEGs were ranked based on their average log2 fold change and the resulting gene list served as input for the GSEA analysis.

Results

Engineering and expansion of CD19- and R110-CAR T cells by LV transduction versus SB transposition

We used two constructs with potential applicability in CLL: An anti-CD19 CAR sequence containing 4-1BB and CD3ζ and a CAR sequence against the CLL neoantigen IGLV3-21^{R110} containing the same elements (Figure 1A). Both sequences were used to construct human T cells expressing the respective CAR either by LV transduction or by SB transposition (Figure 1B). We compared LV- and SB-manufactured CAR T cells derived from healthy donor blood. Despite the cell damage caused by the electroporation procedure for the SB-engineered products, T cell expansion and cell viability recovered within the first week. Figure 1C shows the gating scheme for CAR-expressing T cells using

the scFv-linker as detection marker. The CAR was expressed by approximately 40% of transduced or electroporated T cells two weeks from manipulation (Figure 1D). With SB transposition, we achieved somewhat lower percentages of CAR expression when CLL-derived T cells were used, potentially due to their greater fragility (Figure 1D). scFv membrane density was estimated based on flow cytometry measured mean fluorescence intensity (MFI) of the CAR linker. After stable integration, scFv densities showed no consistent differences between SB- versus LV-manufactured CAR T cells (Figure 1E). R110-CAR expression was, however, consistently lower compared to CD19-CAR expression in both SB- and LV-manufactured products (Figure 1E).

CD4/CD8 distribution and differentiation stages of anti-CD19 and anti-R110 CAR T cells according to mode of production

Equal production media were used for LV- and SB-manufacturing. These contained IL-15 to maintain less differentiated subpopulations because these are believed to better persist in patients (21, 22). While LV-manufacturing resulted in a $CD4^+$ dominant product, SB-manufacturing showed a shift towards $CD8^+$ T cells upon expansion consistent with a previous study (Figure 2A and B) (23). The CD8 shift was more pronounced with anti-R110 CAR T cells.

LV- and SB-production modes showed differences in T cell differentiation states of CAR products derived from the same T cell source (Figure 2C). While SB-manufactured products consisted essentially of a naïve-like T cell phenotype ($CD45RA^+$, $CCR7^+$), LV-manufactured CAR T cells showed a spectrum of $CD4^+$ differentiation stages including terminally differentiated cells ($CD45RA^+$, $CCR7^-$) (Figure 2C). Overall, $scFv^-$ T cells better retained the composition of T cell subtypes over time. Figure 2D shows integrated statistics of differentiation stages in T cells derived from a healthy donor and a CLL patient.

Tonic CAR signaling and co-inhibition in SB- and LV-manufactured products

Interestingly, we observed that in the absence of target cells or antigen, scFv$^+$ CD4$^+$ T cells manufactured with SB showed an increase of the early activation marker CD69 compared to LV-generated CAR T cells as an indication of tonic CAR signaling (Figure 3A). This was more consistently detected for the R110-CAR T cell product. An increase of CD69 was also observed in scFv$^+$ CD8$^+$ cells regardless of the manufacturing mode.

Next, we asked whether tonic CAR signaling leads to killing of bystander antigen-negative cells. We, therefore, calculated the ratio of specific killing by co-culturing different batches of R110- and CD19-CAR T cells with the antigen-positive NALM-6 cell line transduced with the LeGO-iZeo2 lentiviral vector encoding IGLV3-21^{R110} (NALM-6-R110) and the K562 cell line which is negative for CD19 and the R110 neoepitope (Figure 3B). R110-CAR T cells showed somewhat lower rates of specific killing with more background killing of antigen-negative cells compared to CD19 CAR T cells but this was not associated with production mode (Figure 3C).

Next, we explored whether antigen-independent CD69 upregulation was accompanied by expression of other activation or co-inhibition markers. Therefore, we recorded expression of the classical T cell exhaustion markers PD-1, TIM-3 and LAG-3 in CAR T cells that were cultured without exposure to antigen or target cell line. Measurements were performed between day 9 and day 30 in order to follow dynamics over time. Different marker expression was observed depending on the construct and manufacturing mode as shown in Figure 3D and Supplementary Figure 1. While SB-manufactured products expressed slightly more TIM-3, there were more pronounced differences in PD-1 and LAG-3 expression between production modes. SB-manufactured T cells showed considerably lower PD-1 expression while exhibiting high levels of LAG-3 without antigen encounter. In contrast, LV-manufactured products showed higher PD-1 levels, but instead low LAG-3. When visualizing marker expression by tSNE, LAG-3 expression was virtually restricted to

CD8$^+$ subsets, while PD-1 was more expressed on CD4$^+$ cells and especially in the LV-manufactured products (Figure 3E). Overall, SB-manufactured T cells showed the highest LAG-3 expression in almost all CD8$^+$ cells while lacking PD-1 expression.

Single-cell RNA sequencing of SB- and LV-produced CAR T cells

To investigate the impact of CAR T cell manufacturing methods on the cellular states of engineered T cells, we performed integrated single-cell RNA and single-cell TCR sequencing on CD3-sorted CAR T cell cultures. These cultures included R110- and CD19-CAR T cells produced via SB and LV systems from both a healthy donor and a CLL patient. Untransduced T cells (UTDs) from SB production served as controls. Samples were collected on day 21 of production, yielding a total recovery of 67,799 cells (mean per sample 6,780; range 4,102-8,847) that passed quality thresholds, covering the major T cell subsets (CD4$^+$, CD8$^+$, and γδ T cells; Figure 4A, B, C). Using standard surface markers and references from published single-cell atlases, we identified a core CD4$^+$ cluster with subsets displaying naïve (*CD27*, *CCR7*, *SELL*, *TCF7*), regulatory (*IL2RA*, *FOXP3*, *RTKN2*), and memory-like (*ITGB1*) signatures (Figure 4A, B). A proliferation-associated cluster included both CD4$^+$ and naïve-like CD8$^+$ T cells (*MKI67*, *SOX4*). CD4$^+$ and CD8$^+$ T cells were further classified into central memory-like and effector memory-like subsets based on markers such as *CD27*, *GZMK*, *GZMB*, *KLRF1*, *CCR7*, *SELL*, and *LEF1* (Figure 4A, B). In addition, we identified a cluster of memory-like CD4$^+$ T cells with T regulatory cell (T_{reg})/effector-like features (*FOXP3*, *KLRB1*, *ITGB1*), including cells expressing the MAIT cell marker gene *SLC4A10*. We also detected γδ T cells with both naïve-like and effector-like characteristics (*TRDC*, *TRGC1*, *GZMB*, *GZMK*; Figure 4A, B). While all clusters were found with both CAR constructs and production modes, SB-manufactured T cells showed a trend towards expanded proliferative CD4$^+$/CD8$^+$ γδ T cells with high expression of *KLRF1* (proliferation cluster 2, Figure 4A, B). Additionally, γδ T cells and

$CD8^+$ T cells were more prevalent in the SB product, while the LV product contained a higher proportion of $CD4^+$ T cells consistent with flow cytometry (Figure 4C).

Due to overlapping signatures in the overall $CD4^+$ and $CD8^+$ T cell data, we analyzed these subsets separately after reclustering (Figure 4D, E). Based on conventional T cell markers, cluster-specific differentially expressed genes, and published gene signatures for blood-derived T cells, we identified proliferating cells as well as naïve-like and memory-like subsets within both $CD4^+$ and $CD8^+$ populations (Figure 4D, E; Supplementary Figure 2A, B). CAR positive T cells expressing scFv were found across $CD4^+$ and $CD8^+$ clusters, particularly enriched in proliferating and naïve-like subsets, with fewer in memory-like subsets (Figure 4F, G).

In line with the detected $CD45RA^+CCR7^+$ surface patterns (Figure 2C), SB-manufactured CAR T cells exhibited slightly higher expression of markers associated with stem cell-like memory T cells (T_{scm}; *FAS* (CD95), *IL2RB*, *CCR7*, *BCL2*), but did not display differences to LV-manufactured cells according to a global established T_{scm} signature (Figure 4H, I). CAR T cells, regardless of production method, showed limited effector memory (T_{em}) signatures and some central memory (T_{cm}) expression (Figure 4I). In both $CD4^+$ and $CD8^+$ CAR T cells, co-inhibition markers *LAG3* and *HAVCR2* (TIM-3) were considerably elevated compared to T cells not carrying the CAR (Figure 4J). SB-manufactured R110 CAR T cells showed more *LAG3* and *HAVCR2* transcripts compared to SB-manufactured CD19 CAR T cells (Figure 4K, mind different scales).

Pathway analysis in SB- and LV-produced CAR T cells

Next, we tested wheter the SB and LV production modes resulted in activation or suppression of specific pathways. For this, we calculated differentially expressed genes (DEGs) in SB- and LV-manufactured products for the $CD4^+$ $scFv^+$ and $CD8^+$ $scFv^+$ populations as well as the $scFv^-$ bystander cells (Figure 5). Interestingly, across all DEG

analyses, scFv$^+$ cells consistently yielded higher numbers of DEGs (Figure 5A, D). Independent of scFv expression, CD4$^+$ T cells from the SB batch were characterized by increased expression of the chemokine *CCL5* (RANTES), the proliferative transcription factor *HDGLF3* and of cytotoxicity markers (*GZMA* and *GZMB*) including the transcription factor *BHLHE40* that is crucial for regulating T cell effector functions (24) (Figure 5A). Gene set enrichment analysis revealed that T cells from the SB production had higher expression of proinflammatory genes related to TNF, interferon (IFN) and JAK-STAT signaling (Figure 5B). In contrast, SB-manufactured T cells displayed decreased levels of genes for cell cycle control, replication and proliferation (*MYB*, *PCLAF*, *H2AFZ*, *HIST1H1A*) (Figure 5A, B). The scFv$^+$ CD4$^+$ T cells from the SB production were especially characterized by the enrichment of genes (*DDX60*, *DDX3X*, *TBK1*) that act in the RNA/DNA-sensing RIG-I and TLR signaling pathways including the pivotal mediators and effectors from the NFκB (*IKBKE*, *TRAF2*, *RELA*) and interferon signaling pathways (*IRF3*, *IRF7*, *IFIH1*, *ISG15*) (Figure 5B, C). In addition, CD4$^+$ T cells from the SB-batches also had high levels of the E3 ISGylation ligase 5 (*HERC5*) that mediates activating ISGylation of the cytosolic DNA sensor STING (25) (Figure 5A). Notably, we did not observe enriched RIG-I and TLR gene signatures in CD8$^+$ CAR T cells from the SB production (Figure 5D, E). Instead, CD8$^+$ scFv$^+$ T cells were characterized by increased expression of *CCL3*, *CCL4* and the FYN/CSK/Abl interacting transmembrane adatpor protein *PAG1* that negatively regulates T cell activation and is linked to anergy (26, 27) (Figure 5D). Moreover, CD8$^+$ scFv$^+$ cells displayed enriched p53 pathway signatures, which may be associated with CD8$^+$ T cell exhaustion (28), and had increased levels of *LAG3* as compared to cells from the LV production (Figure 5D). CD8$^+$ CAR T cells from the SB production shared the general enrichment of pro-inflammatory signatures with their CD4$^+$ counterparts (Figure 5D, E). To validate the observed RIG-I/TLR signatures and determine whether they are induced by RNA or DNA in the transfection process, we electroporated

$CD3^+$ T cells with either the SB mRNA or the CAR DNA constructs alone. Surface marker expression was quantified after 7 days using flow cytometry. The data revealed that, particularly after mRNA delivery, the surface expression of CD69, PD-1, TIM-3, and LAG-3 significantly increased (Figure 5F).

Donor cell constitution impacts transcriptomic signatures of CAR T cells

To test for donor-dependent transcriptome differences, we separated the single-cell data set into HD- and CLL-derived cells (Figure 6A, C). While all defined T cell subpopulations (Figure 4) encompassed cells from both donors (Figure 6A, B), the CLL-derived T cell pools had lower numbers of proliferating cells, but higer numbers of γδ, $CD4^+$, $CD8^+$ T_{em} and $CD4^+$ memory T cells (Figure 6A, B). CLL-derived products had generally increased transcipt levels of *LAG3*, *CD69*, *ID2*, *SLAMF7* several chemokines and lncRNAs as well as HLA class molecules and cytotoxicity markers (Figure 6A, C). In contrast, genes related to cell cycle control and proliferation exhibited pervasively lower transcript levels as compared to HD-derived T cells (Figure 6A, C). Within the reclustered $CD4^+$ and $CD8^+$ subsets (Figure 4D, E) we detected an enrichment of memory-like cells in CLL-derived T cells independent of production mode, while HD-derived T cells were more enriched for proliferating cells (Figure 6D).

Finally, we tested for donor-dependent differences in activation/co-inhibition markers. As compared to HD-derived cells, the SB-associated increase of *LAG3* expression was more pronounced in $CD4^+$ than in $CD8^+$ $scFv^+$ T cells derived from CLL patients (Figure 6E). In addition, we observed higher levels of *PDCD1*, *TIGIT* and *TOX2* in CLL-derived $CD4^+$ T cells with scFv expression from the SB production (Figure 6E). CAR T cells from the LV production had lower levels of these markers and showed no clear donor-dependent differences (Figure 6E).

TCR repertoire analysis of CAR T cells

Single-cell TCR analysis demonstrated polyclonality across all products, with no notable differences between CAR T cells manufactured via SB and LV methods. T cell characteristics, however, varied significantly with the donor source. CAR T products derived from the CLL donor exhibited lower T cell richness and diversity compared to those from the HD, highlighting a restriction in the CLL donor's T cell repertoire (Figure 7A). This limitation was further confirmed by TCR repertoire overlap analysis, which revealed substantial clonal overlap between the CLL donor's CAR T products, in contrast to the HD-derived products, which showed minimal clonal overlap (Figure 7B). TRA and TRB gene analyses identified a broad spectrum of gene usage in both donors, with some patterns specific to each donor (Figure 7C). This trend was reflected in a principal component analysis (PCA) of TRBVJ gene usage, where CAR T cell products from each donor clustered together. No distinct differences were observed based on production method or CAR binding moiety (Figure 7D).

Discussion

T cell dysfunction is one of the major roadblocks in the development and application of CAR T cell therapies (7). There is only scarce data on how the production mode and the binding moiety may impact CAR T cell phenotypes. Here, we provide a head-to-head comparison of different production modes – lentiviral transfection and sleeping beauty transposition – of R110- and CD19-directed CAR T cells with a focus on T cell activation and co-inhibition marker expression.

In our study, we demonstrate that different CAR constructs exhibit distinct patterns of marker expression for T cell activation and co-inhibition. Notably, we observed substantial differences between SB and LV production methods, even when using identical CAR sequences, T cell donors, and culture conditions – factors known to critically impact the

final CAR T cell product (21). Our data suggest that especially the delivery of SB mRNA is a dominant driver of the exhausted-like phenotypes by eliciting intracellular nucleic acid-sensing pathways like RIG-I. Interestingly, upregulation of RIG-I signaling has been reported in terminally exhausted $CD8^+$ T cells and was linked to reduced $CD8^+$ T cell effector functions in tumor-infiltrating lymphocytes (29). Also, other product-defining features were significantly affected by the production mode, such as CD4/8 ratio, differentiation stage or CD69 expression as a marker for antigen-independent tonic activation. These findings are crucial as they suggest that the optimization of CAR constructs extends beyond the design of co-stimulatory domains or the configuration of the binding moiety supporting that each construct must also be rigorously tested under various manufacturing conditions.

In a related approach, a previous study compared the phenotypes of CD19-targeting CAR T cells either manufactured using electroporation and the PiggyBac transposase system or produced by lentiviral transduction (30). The authors noted higher CAR-density and cytokine release in CAR T cells generated with the transposase system, but no significant differences regarding CD69 or PD-1 surface expression or anti-tumor efficacy in a murine xenograft model (30). CAR T cells produced with the transposase system displayed lower frequencies of T_{cm} and T_{em} phenotypes as their lentiviral counterparts and had higher expression of genes related to immunological and inflammatory pathways as shown in our study (30). However, their analyses were restricted to the first week after CAR T production (30).

There is some data linking CAR T cell phenotypes to efficacy outcomes of CAR T cells in patients. While some studies suggested that a balanced ratio of CD4 and CD8 cells in the product would support persistence and eradication of the malignant clone in patients (31, 32), others did not support this conclusion (8). Moreover, in one study early memory T cell differentiation in the CAR T cell product was found to correlate with better responses while

an effector or exhausted T cell differentiation was not (8). In another study, peak CAR T cell detection in patients correlated with the percentage of a naïve CAR^+ $CD8^+CD45RA^+CCR7^+$ T cell subset in the CAR T cell product (33). Furthermore, the percentage of $PD\text{-}1^+CD8^+$ CAR T cells coexpressing either TIM-3 or LAG-3 correlated with a lower response to therapy (8). CD62L (*SELL*), also known as L-selectin, is another marker of naïve T cells, including stem cell memory T cells, but also central memory T cells. Its enhanced expression was shown to lead to better control of tumor growth in an in vivo model and its expression level was associated with a better ex vivo expansion (34-36). Overall, T cell subset distribution and co-inhibitory receptor expression as well as prior antigen encounter influences outcomes with CAR T cells (21, 36, 37), suggesting that the differences associated with production mode and CAR specificity seen in our study may be of clinical relevance.

The determinants of T cell dysfunction in the setting of CAR T cells are still rather ill defined. T cell exhaustion is considered the result of continuous exposure to antigen (7, 38) but may also occur without antigen exposure in the case of CAR T cells, e.g. by self-aggregation of the CAR resulting in tonic signaling (7). It has been assumed that tonic signaling could not only be a feature of the CAR sequence itself, but also a function of CAR membrane density. To this end, “self-driving” armored CAR T cells that upregulate CAR expression only in case of antigen encounter were developed and tested preclinically (39). As opposed to this assumption, we found that the pattern of high LAG-3 expression was not associated with higher expression of CAR molecules. In contrast, we observed higher basal LAG-3 expression in SB-manufactured R110-CAR T cells that showed much lower CAR density than CD19-directed CAR T cells. This suggests that – at least in our model – high CAR expression is not a critical inducer of tonic CAR signaling.

We observed a low percentage of $scFv^+$ T cells and a depletion of proliferative T cell clusters in CAR T cells derived from the CLL donor. These effects were more pronounced

in SB-manufactured products, suggesting that the stress associated with SB transposition may further impact the already fragile T cells from patients, thereby impairing their proliferative capacity. In conditions like CLL, where T cell defects are well-documented, it will be essential to investigate this further to optimize transgene delivery and achieve a cell product that can proliferate and persist effectively in patients.

In summary, while CAR T cells hold great promise in oncology, T cell functionality remains a critical challenge, particularly in the autologous setting. Addressing this issue is essential for enhancing the efficacy and expanding the applicability of CAR T cell therapies across a broader range of cancers.

Acknowledgements

This study was partially funded by SinABiomedics as well as the innovation focus cell therapies at the University Hospital of Base and the Swiss National Science Foundation (SNSF) [10.001.762] (to M.B.).

Author contributions

Idea & design of research project: MB; Supply of critical material (e.g. patient material, cohorts): MB; Establishment of Methods: SS, CS, PBS, AZ, CF, HL; Experimental work: SS, CS, PSB, CF, AZ, NF; Analysis and interpretation of primary data: MB, CS, SS, SA, PBS; Drafting of manuscript: MB, CS, SS. All authors reviewed and revised the manuscript.

Conflict of interest statement

MB is inventor of patent EP22186810.2. All other authors disclose no potential conflicts of interest.

Data availability statement

Single Cell Sequencing data has been deposited at XXX.

Code availability

No code has been developed for this study.

Supplementary Table 1. Antibodies used for flow cytometry.

Target	Conjugated fluorophore	Supplier	Reference Number	Host species	Comment
EGFRt	NA	Merck (Darmstadt, Germany)	NA (Erbitux®)	NA (Humanized)	Cetuximab, used to detect the spliced off truncated EGFR as a surrogate for the CAR construct. Diluted at 1:500.
Human IgG	FITC	Thermo Fisher Scientific	F4512-1ML	Rabbit	Used to detect Cetuximab/anti-EGFR-antibody. Diluted at 1:1000.
Whitlow/218-scFv-Linker	NA	Cell Signaling Technologies (Danvers, MA, USA)	57710S	Rabbit	Used to detect anti-CD19 CAR.
G4S-scFv-Linker	NA	Cell Signaling Technologies	71645S	Rabbit	Used to detect anti-R110 CAR.
Rabbit IgG	AF488	Cell Signaling Technologies	4412S	Goat	Used to detect anti-scFv-Linker-antibodies.
CD19	PE/Dazzle	BioLegend (San Diego, CA, USA)	302251	Mouse	
CD19	APC	BioLegend	302212	Mouse	
CD3	AF700	BioLegend	300424	Mouse	
CD3	FITC	BD BioSciences (Franklin Lanes, NJ, USA)	345763	Mouse	Used for sorting prior to single-cell sequencing.
CD4	BV605	BioLegend	344646	Mouse	
CD8	BV650	BioLegend	344729	Mouse	
PD-1	PE	BioLegend	329905	Mouse	
LAG-3	PE/Cy7	BioLegend	369309	Mouse	
TIM-3	APC/Cy7	BioLegend	345025	Mouse	
CD69	APC	BioLegend	985206	Mouse	
CCR7	PerCP	Invitrogen (Carlsbad, CA, USA)	46-1979-42	Rat	
CD45RA	APC	Invitrogen	47-0458-42	Mouse	
IGLV3-21^{R110} light chain	PE	AVA LifeScience (Denzlingen, Germany)	AVA-D01-PE/01P0150	Mouse	

References

1. June CH, and Sadelain M. Chimeric Antigen Receptor Therapy. *N Engl J Med.* 2018;379(1):64-73.
2. Cappell KM, and Kochenderfer JN. Long-term outcomes following CAR T cell therapy: what we know so far. *Nat Rev Clin Oncol.* 2023;20(6):359-71.
3. Gandara C, Affleck V, and Stoll EA. Manufacture of Third-Generation Lentivirus for Preclinical Use, with Process Development Considerations for Translation to Good Manufacturing Practice. *Hum Gene Ther Methods.* 2018;29(1):1-15.
4. White M, Whittaker R, Gandara C, and Stoll EA. A Guide to Approaching Regulatory Considerations for Lentiviral-Mediated Gene Therapies. *Hum Gene Ther Methods.* 2017;28(4):163-76.
5. Kebriaei P, Singh H, Huls MH, Figliola MJ, Bassett R, Olivares S, et al. Phase I trials using Sleeping Beauty to generate CD19-specific CAR T cells. *J Clin Invest.* 2016;126(9):3363-76.
6. Maiti SN, Huls H, Singh H, Dawson M, Figliola M, Olivares S, et al. Sleeping beauty system to redirect T-cell specificity for human applications. *J Immunother.* 2013;36(2):112-23.
7. Kouro T, Himuro H, and Sasada T. Exhaustion of CAR T cells: potential causes and solutions. *J Transl Med.* 2022;20(1):239.
8. Fraietta JA, Lacey SF, Orlando EJ, Pruteanu-Malinici I, Gohil M, Lundh S, et al. Determinants of response and resistance to CD19 chimeric antigen receptor (CAR) T cell therapy of chronic lymphocytic leukemia. *Nat Med.* 2018;24(5):563-71.
9. Long AH, Haso WM, Shern JF, Wanhainen KM, Murgai M, Ingaramo M, et al. 4-1BB costimulation ameliorates T cell exhaustion induced by tonic signaling of chimeric antigen receptors. *Nat Med.* 2015;21(6):581-90.
10. Gomes-Silva D, Mukherjee M, Srinivasan M, Krenciute G, Dakhova O, Zheng Y, et al. Tonic 4-1BB Costimulation in Chimeric Antigen Receptors Impedes T Cell Survival and Is Vector-Dependent. *Cell Rep.* 2017;21(1):17-26.
11. Watanabe N, Bajgain P, Sukumaran S, Ansari S, Heslop HE, Rooney CM, et al. Fine-tuning the CAR spacer improves T-cell potency. *Oncoimmunology.* 2016;5(12):e1253656.
12. Ajina A, and Maher J. Strategies to Address Chimeric Antigen Receptor Tonic Signaling. *Mol Cancer Ther.* 2018;17(9):1795-815.
13. Markl F, Schultheiss C, Ali M, Chen SS, Zintchenko M, Egli L, et al. Mutation-specific CAR T cells as precision therapy for IGLV3-21(R110) expressing high-risk chronic lymphocytic leukemia. *Nat Commun.* 2024;15(1):993.
14. Belkina AC, Ciccolella CO, Anno R, Halpert R, Spidlen J, and Snyder-Cappione JE. Automated optimized parameters for T-distributed stochastic neighbor embedding improve visualization and analysis of large datasets. *Nat Commun.* 2019;10(1):5415.
15. Schultheiss C, Paschold L, Willscher E, Simnica D, Wostemeier A, Muscate F, et al. Maturation trajectories and transcriptional landscape of plasmablasts and autoreactive B cells in COVID-19. *iScience.* 2021;24(11):103325.
16. Schultheiss C, Paschold L, Mohebiany AN, Escher M, Kattimani YM, Muller M, et al. A20 haploinsufficiency disturbs immune homeostasis and drives the transformation of lymphocytes with permissive antigen receptors. *Sci Adv.* 2024;10(34):eadl3975.
17. Hao Y, Hao S, Andersen-Nissen E, Mauck WM, 3rd, Zheng S, Butler A, et al. Integrated analysis of multimodal single-cell data. *Cell.* 2021;184(13):3573-87 e29.
18. Borcherding N, Bormann NL, and Kraus G. scRepertoire: An R-based toolkit for single-cell immune receptor analysis. *F1000Res.* 2020;9:47.

19. Korsunsky I, Millard N, Fan J, Slowikowski K, Zhang F, Wei K, et al. Fast, sensitive and accurate integration of single-cell data with Harmony. *Nat Methods.* 2019;16(12):1289-96.
20. Andreatta M, and Carmona SJ. UCell: Robust and scalable single-cell gene signature scoring. *Comput Struct Biotechnol J.* 2021;19:3796-8.
21. Lopez-Cantillo G, Uruena C, Camacho BA, and Ramirez-Segura C. CAR-T Cell Performance: How to Improve Their Persistence? *Front Immunol.* 2022;13:878209.
22. Chan JD, Lai J, Slaney CY, Kallies A, Beavis PA, and Darcy PK. Cellular networks controlling T cell persistence in adoptive cell therapy. *Nat Rev Immunol.* 2021;21(12):769-84.
23. Magnani CF, Gaipa G, Lussana F, Belotti D, Gritti G, Napolitano S, et al. Sleeping Beauty-engineered CAR T cells achieve antileukemic activity without severe toxicities. *J Clin Invest.* 2020;130(11):6021-33.
24. Salmon AJ, Shavkunov AS, Miao Q, Jarjour NN, Keshari S, Esaulova E, et al. BHLHE40 Regulates the T-Cell Effector Function Required for Tumor Microenvironment Remodeling and Immune Checkpoint Therapy Efficacy. *Cancer Immunol Res.* 2022;10(5):597-611.
25. Qin Y, Wang M, Meng X, Wang M, Jiang H, Gao Y, et al. ISGylation by HERCs facilitates STING activation. *Cell Rep.* 2024;43(5):114135.
26. Davidson D, Bakinowski M, Thomas ML, Horejsi V, and Veillette A. Phosphorylation-dependent regulation of T-cell activation by PAG/Cbp, a lipid raft-associated transmembrane adaptor. *Mol Cell Biol.* 2003;23(6):2017-28.
27. Saibil SD, Deenick EK, and Ohashi PS. The sound of silence: modulating anergy in T lymphocytes. *Curr Opin Immunol.* 2007;19(6):658-64.
28. Barili V, Fisicaro P, Montanini B, Acerbi G, Filippi A, Forleo G, et al. Targeting p53 and histone methyltransferases restores exhausted CD8+ T cells in HCV infection. *Nat Commun.* 2020;11(1):604.
29. Duan X, Hu J, Zhang Y, Zhao X, Yang M, Sun T, et al. RIG-I is an intracellular checkpoint that limits CD8(+) T-cell antitumour immunity. *EMBO Mol Med.* 2024.
30. Niu A, Zou J, Hu X, Zhang Z, Su L, Wang J, et al. Differences in the phenotypes and transcriptomic signatures of chimeric antigen receptor T lymphocytes manufactured via electroporation or lentiviral transfection. *Front Immunol.* 2023;14:1068625.
31. Turtle CJ, Hanafi LA, Berger C, Gooley TA, Cherian S, Hudecek M, et al. CD19 CAR-T cells of defined CD4+:CD8+ composition in adult B cell ALL patients. *J Clin Invest.* 2016;126(6):2123-38.
32. Sommermeyer D, Hudecek M, Kosasih PL, Gogishvili T, Maloney DG, Turtle CJ, et al. Chimeric antigen receptor-modified T cells derived from defined CD8+ and CD4+ subsets confer superior antitumor reactivity in vivo. *Leukemia.* 2016;30(2):492-500.
33. Xu Y, Zhang M, Ramos CA, Durett A, Liu E, Dakhova O, et al. Closely related T-memory stem cells correlate with in vivo expansion of CAR.CD19-T cells and are preserved by IL-7 and IL-15. *Blood.* 2014;123(24):3750-9.
34. Watson HA, Durairaj RRP, Ohme J, Alatsatianos M, Almutairi H, Mohammed RN, et al. L-Selectin Enhanced T Cells Improve the Efficacy of Cancer Immunotherapy. *Front Immunol.* 2019;10:1321.
35. Kasuya H, Zhang H, Ito Y, Yoshikawa T, Nakashima T, Li Y, et al. High CD62L expression predicts the generation of chimeric antigen receptor T cells with potent effector functions. *Int Immunol.* 2024;36(7):353-64.
36. Brown CE, Hibbard JC, Alizadeh D, Blanchard MS, Natri HM, Wang D, et al. Locoregional delivery of IL-13Ralpha2-targeting CAR-T cells in recurrent high-grade glioma: a phase 1 trial. *Nat Med.* 2024;30(4):1001-12.
37. DeGolier KR, Danis E, D'Antonio M, Cimons J, Yarnell M, Kedl RM, et al. Antigen experience history directs distinct functional states of CD8(+) CAR T cells during the antileukemia response. *Nat Immunol.* 2025;26(1):68-81.

38. Wherry EJ, and Kurachi M. Molecular and cellular insights into T cell exhaustion. *Nat Rev Immunol*. 2015;15(8):486-99.
39. Webster B, Xiong Y, Hu P, Wu D, Alabanza L, Orentas RJ, et al. Self-driving armored CAR-T cells overcome a suppressive milieu and eradicate CD19(+) Raji lymphoma in preclinical models. *Mol Ther.* 2021;29(9):2691-706.

Figure legends

Figure 1. Development of a chimeric antigen receptor (CAR) T cell targeting either CD19 or the IGLV3-21^{R110} neoepitope by LV transfection and SB transposition. (A) Schematic representation of the CD19 and IGLV3-21^{R110} (R110) CAR T targeting principle against chronic lymphocytic leukemia (CLL) cells. BCR, B cell receptor. scFv, single-chain variable fragment. **(B)** Schematic representation of the CAR T cell production workflow by LV transfection and SB transposition. **(C)** Gating strategy to determine CAR expression on T cells by flow cytometry. **(D)** Percentage of CAR-positive T cells determined by scFv expression using flow cytometry over the course of four weeks. **(E)** CAR density on T cells determined by the mean fluorescence intensity (MFI) of the scFv using flow cytometry over the course of four weeks. Bars represent the mean ± SD of pooled samples of healthy donor HD175 and CLL patient CLL456 measured in duplicates.

Figure 2. Characterization of the CD4 to CD8 ratio and T cell differentiation of CD19 and R110 targeting CAR T cells. (A) Representative image of the distribution of CD4$^+$ and CD8$^+$ CAR T cells on day 16. **(B)** Calculated CD4$^+$ to CD8$^+$ ratio of scFv$^{+/-}$ CAR T cells over the course of four weeks. **(C)** Representative T cell differentiation pattern of scFv$^{+/-}$ and CD4$^+$/CD8$^+$ CAR T cells derived from HD175 measured in technical duplicates by flow cytometry after 9 and 30 days. **(D)** Summarized results of the T cell differentiation pattern of pooled scFv$^{+/-}$ and CD4$^+$/CD8$^+$ CAR T cell samples of HD175 and CLL456, separated into CD4$^+$ and CD8$^+$ T cells and according to their scFv expression.

Figure 3. Expression patterns of activation and co-inhibition markers in healthy donor and CLL patient-derived CAR T cells by flow cytometry. (A) CD69 surface expression in either scFv$^+$,CD4$^+$ or scFv$^+$,CD8$^+$ CAR T cells over the course of four weeks. Bars represent the mean ± SD of pooled samples of HD175 and CLL456 measured in duplicates. **(B)** Representative flow cytometry image of target epitope expression in K562 and NALM-6-R110 cells. **(C)** Pooled results of in vitro coculture assays indicating the killing of CD19$^+$, IGLV3-21^{R110+} NALM-6-R110 target cells in relation to CD19$^-$,IGLV3-21^{R110-} K562 non-target cells. Bars represent the mean ± SD of pooled experiments. **(D)** Histogram of the PD-1, TIM-3 and LAG-3 expression in CD3$^+$ T cells (HD175) on day 9. **(E)** Visualization of the CD4, CD8, PD-1 and LAG-3 distribution pattern of CD3$^+$ T cells (HD175) on day 16. Technical duplicate measurements were concatenated and tSNE analysis performed with standard settings.

Figure 4. Single-cell RNA sequencing analysis of CD3$^+$ T cells from SB and LV production pools. (A) Uniform manifold and approximation projection (UMAP) plot of CD3$^+$ T cells from the SB and LV production pools. Stacked bar plots display the cluster cell distribution based on CAR T production batches (including UTD control cells) or production mode (SB: sleeping beauty transposition; LV: lentiviral transduction) for all CD3$^+$ T cells and CAR T cells only (scFv$^+$ cells). **(B)** Heatmap of average normalized expression for conventional T cell marker genes in each cluster. **(C)** UMAP plot showing *CD4*, *CD8A* and *TRDC* expression in CD3$^+$ T cells with respect to CAR T production mode. **(D)** UMAP plot of CD4$^+$ T cells after re-clustering. Expression of T cell markers and selected cluster-defining genes as dot plot grouped by production mode. Dotted lines indicate proliferating T cell clusters. **(E)** UMAP plot of CD8$^+$ T cells after re-clustering. Expression of T cell markers and selected cluster-defining genes as dot plot grouped by production mode. Dotted lines indicate proliferating T cell clusters. **(F)** UMAP plot of CD4$^+$

and $CD8^+$ T cell subsets with marked $scFv^+$ T cells per production mode. **(G)** Proportion of $scFv^+$ cells per cluster in (F). **(H)** Violin plots showing expression of marker genes for stem cell-like T memory cells (T_{scm}) in $scFv^+$ cells from the SB and LV production. **(I)** UMAP plot showing enrichment of gene signature scores for the indicated T cell subpopulations depending on production mode. **(J)** Dot plot showing the expression of selected T cell exhaustion/activation markers in $scFv^{+/-}$ cells. **(K)** Dot plot showing the expression of selected T cell exhaustion/activation markers in $scFv^+$ $CD4^+$ or $CD8^+$ T cells depending on production mode.

Figure 5. Characterization of production protocol-specific transcriptomic signatures in $CD3^+$ T cells from SB and LV production pools. (A) Volcano plot showing genes differentially expressed (adjusted $P < 0.01$) between SB and LV production modes for $CD4^+$ $scFv^+$ (upper panel) and $CD4^+$ $scFv^-$ T cells (lower panel). **(B)** Gene set enrichment of GSEA/KEGG (upper panel) and GSEA/Hallmark pathways (lower panel) in SB-manufactured $scFv^+$ $CD4^+$ T cells as compared to the LV production. **(C)** Dot plot showing the average normalized expression of genes from the RIG-I receptor signaling gene set in SB- and LV-produced $scFv^+$ $CD4^+$ T cells. **(D)** Volcano plot showing genes differentially expressed (adjusted $P < 0.01$) between SB and LV production modes for $CD8^+$ $scFv^+$ (upper panel) and $CD8^+$ $scFv^-$ T cells (lower panel). **(E)** Enrichment of GSEA/Hallmark pathway genes in SB-manufactured $scFv^+$ $CD8^+$ T cells as compared to the LV production. **(F)** Heatmap displaying surface expression of indicated markers as MFI on day 7 for mono-electroporation of SB mRNA, anti-CD19 or anti-R110 CAR DNA constructs. Control T cells underwent electroporation only.

Figure 6. Analysis of donor-dependent impact on SB- and LV-manufactured CAR T cell transcriptomes. (A) UMAP plot of healthy donor (HD)- or CLL patient-derived $CD3^+$ T cells displaying expression of selected T cell markers. **(B)** Cell numbers in the indicated subpopulations (s. Figure 4) depending on the donor. **(C)** Heatmap showing differential expression of genes between HD-/CLL-derived $CD3^+$ T cells. **(D)** Radar plot displaying the contribution of HD-/CLL-derived $CD4^+$ $scFv^{+/-}$ and $CD8^+$ $scFv^{+/-}$ T cells to the single subsets in the bulk $CD4^+$ and $CD8^+$ populations from the SB and LV production pools. **(E)** Violin plot showing expression of indicated exhaustion/co-inhibition markers in HD-/CLL-derived $CD4^+$ and $CD8^+$ $scFv^+$ T cells.

Figure 7. T cell receptor repertoire analysis of SB- and LV-manufactured CAR T cells. (A) Immune metrics. **(B)** Shared CDR3 sequences between donors and production batches. **(C)** Frequencies of TRBV gene usage. **(D)** PCA of TRBVJ usage.

Supplementary Figure Legends

Supplementary Figure 1. Expression patterns of activation and co-inhibition markers in healthy donor and CLL patient-derived CAR T cells by multicolor flow cytometric analysis. (A) CD69, **(B)** TIM-3, **(C)** LAG-3 and **(D)** PD-1 mean fluorescence intensities (MFI) in CAR T cells separated by CD4, CD8, $scFv^+$ and $scFv^-$ expression. Bars represent the mean ± SD of pooled samples of HD175 and CLL456 measured in duplicates.

Supplementary Figure 2. Top 10 differentially expressed genes per cluster in the $CD4^+$ and $CD8^+$ subsets.

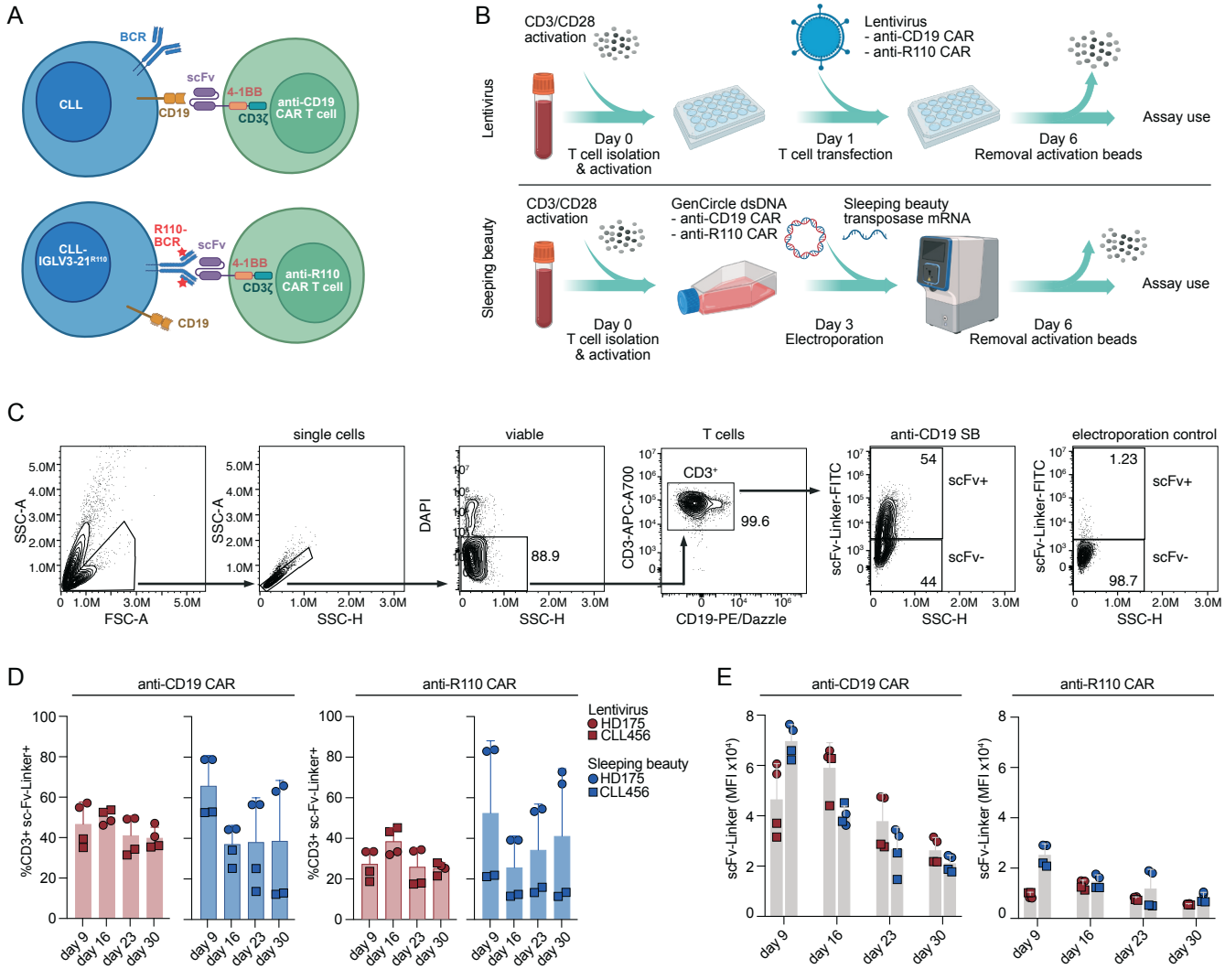
A
BCR
CLL
scFv
CD19
4-1BB
CD3ζ
anti-CD19 CAR T cell
CLL-IGLV3-21R110
R110-BCR
scFv
4-1BB
CD3ζ
anti-R110 CAR T cell
CD19
B
Lentivirus
CD3/CD28 activation
Lentivirus - anti-CD19 CAR - anti-R110 CAR
Day 0 T cell isolation & activation
Day 1 T cell transfection
Day 6 Removal activation beads
Assay use
Sleeping beauty
CD3/CD28 activation
GenCircle dsDNA - anti-CD19 CAR - anti-R110 CAR
Sleeping beauty transposase mRNA
Day 0 T cell isolation & activation
Day 3 Electroporation
Day 6 Removal activation beads
Assay use
C
single cells
viable
T cells
anti-CD19 SB
electroporation control
SSC-A
FSC-A
SSC-H
DAPI
88.9
CD3-APC-A700
CD3+
99.6
CD19-PE/Dazzle
scFv-Linker-FITC
54
scFv+
44
scFv-
1.23
98.7
D
anti-CD19 CAR
anti-R110 CAR
%CD3+ sc-Fv-Linker+
Lentivirus
HD175
CLL456
Sleeping beauty
HD175
CLL456
day 9
day 16
day 23
day 30
E
anti-CD19 CAR
anti-R110 CAR
scFv-Linker (MFI x10⁴)

Figure 1

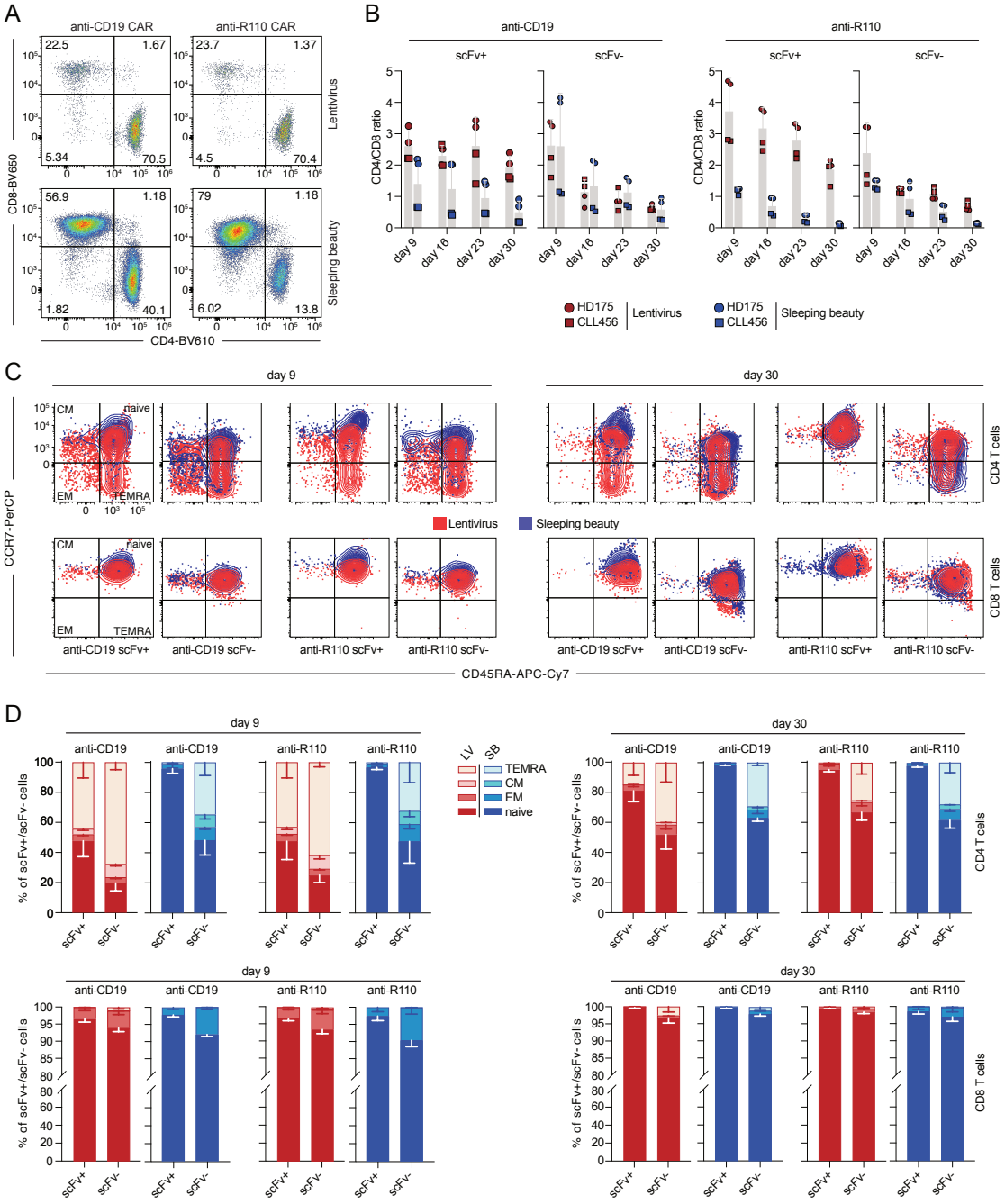
A
anti-CD19 CAR
anti-R110 CAR
Lentivirus
Sleeping beauty
CD8-BV650
CD4-BV610
B
anti-CD19
anti-R110
scFv+
scFv-
CD4/CD8 ratio
day 9
day 16
day 23
day 30
HD175
CLL456
Lentivirus
Sleeping beauty
C
day 9
day 30
CCR7-PerCP
CD45RA-APC-Cy7
CD4 T cells
CD8 T cells
Lentivirus
Sleeping beauty
anti-CD19 scFv+
anti-CD19 scFv-
anti-R110 scFv+
anti-R110 scFv-
CM
naive
EM
TEMRA
D
% of scFv+/scFv- cells
LV
SB
TEMRA
CM
EM
naive

Figure 2

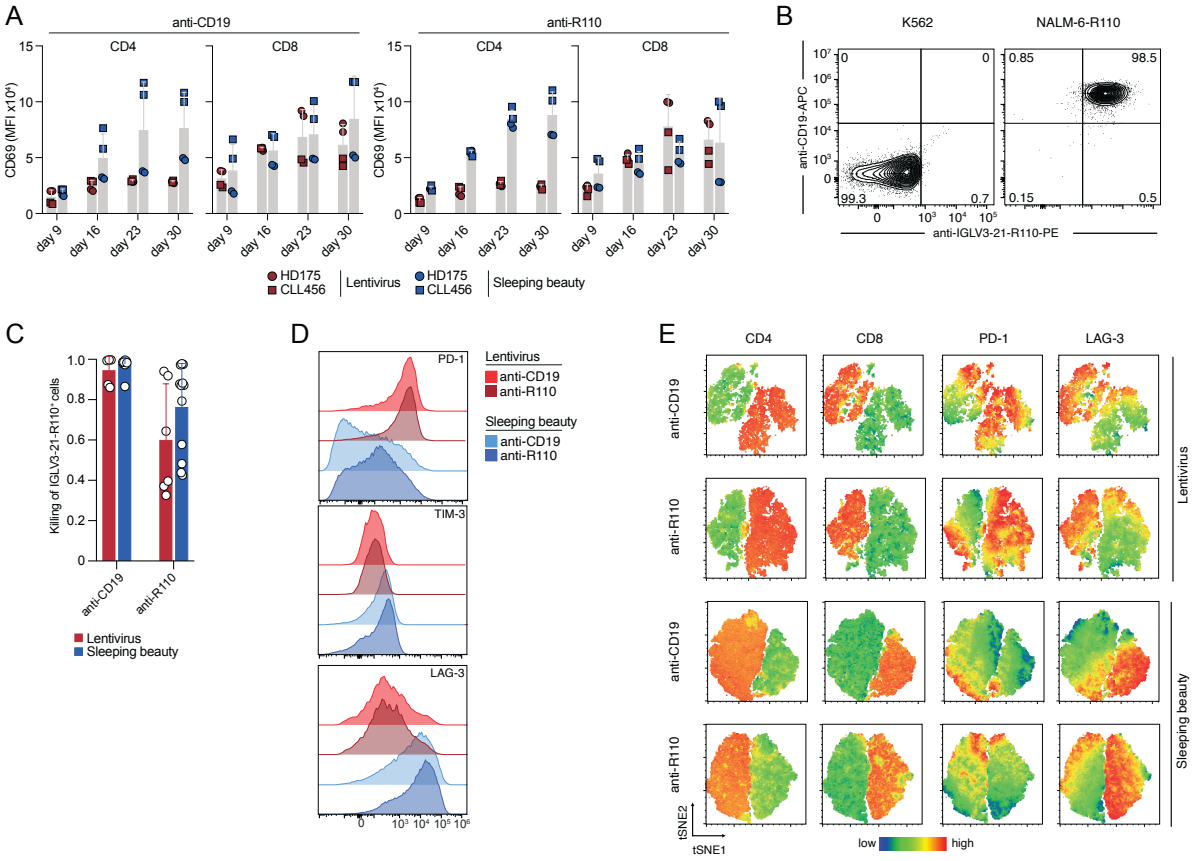
A
anti-CD19
anti-R110
CD4
CD8
CD69 (MFI x10⁴)
day 9
day 16
day 23
day 30
HD175
CLL456
Lentivirus
Sleeping beauty
B
K562
NALM-6-R110
anti-CD19-APC
anti-IGLV3-21-R110-PE
C
Killing of IGLV3-21-R110⁺ cells
anti-CD19
anti-R110
Lentivirus
Sleeping beauty
D
PD-1
TIM-3
LAG-3
Lentivirus
anti-CD19
anti-R110
Sleeping beauty
anti-CD19
anti-R110
E
CD4
CD8
PD-1
LAG-3
anti-CD19
anti-R110
Lentivirus
Sleeping beauty
tSNE2
tSNE1
low
high

Figure3

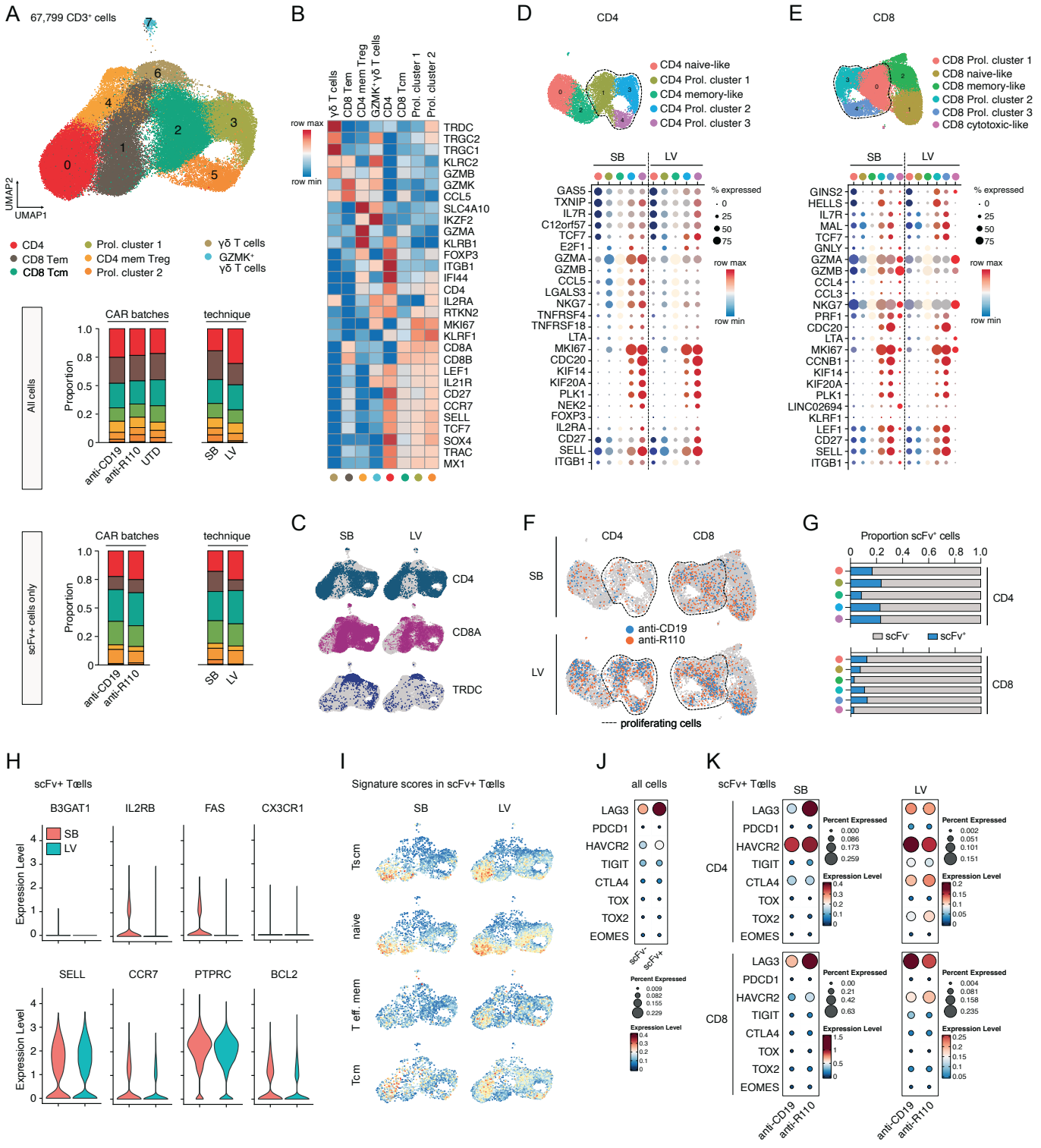
A
67,799 CD3⁺ cells
UMAP2
UMAP1
CD4
CD8 Tem
CD8 Tcm
Prol. cluster 1
CD4 mem Treg
Prol. cluster 2
γδ T cells
GZMK⁺ γδ T cells
All cells
scFv+ cells only
CAR batches
technique
Proportion
anti-CD19
anti-R110
UTD
SB
LV
B
γδ T cells
CD8 Tem
CD4 mem Treg
GZMK⁺γδ T cells
CD4
CD8 Tcm
Prol. cluster 1
Prol. cluster 2
row max
row min
TRDC
TRGC2
TRGC1
KLRC2
GZMB
GZMK
CCL5
SLC4A10
IKZF2
GZMA
KLRB1
FOXP3
ITGB1
IFI44
CD4
IL2RA
RTKN2
MKI67
KLRF1
CD8A
CD8B
LEF1
IL21R
CD27
CCR7
SELL
TCF7
SOX4
TRAC
MX1
C
SB
LV
CD4
CD8A
TRDC
D
CD4
CD4 naive-like
CD4 Prol. cluster 1
CD4 memory-like
CD4 Prol. cluster 2
CD4 Prol. cluster 3
% expressed
row max
row min
GAS5
TXNIP
IL7R
C12orf57
TCF7
E2F1
GZMA
GZMB
CCL5
LGALS3
NKG7
TNFRSF4
TNFRSF18
LTA
MKI67
CDC20
KIF14
KIF20A
PLK1
NEK2
FOXP3
IL2RA
CD27
SELL
ITGB1
E
CD8
CD8 Prol. cluster 1
CD8 naive-like
CD8 memory-like
CD8 Prol. cluster 2
CD8 Prol. cluster 3
CD8 cytotoxic-like
GINS2
HELLS
IL7R
MAL
TCF7
GNLY
GZMA
GZMB
CCL4
CCL3
NKG7
PRF1
CDC20
LTA
MKI67
CCNB1
KIF14
KIF20A
PLK1
LINC02694
KLRF1
LEF1
CD27
SELL
ITGB1
F
CD4
CD8
SB
LV
anti-CD19
anti-R110
proliferating cells
G
Proportion scFv⁺ cells
CD4
CD8
scFv⁻
scFv⁺
H
scFv+ Tcells
B3GAT1
IL2RB
FAS
CX3CR1
SELL
CCR7
PTPRC
BCL2
Expression Level
I
Signature scores in scFv+ Tcells
SB
LV
Tscm
naive
T eff. mem
Tcm
J
all cells
LAG3
PDCD1
HAVCR2
TIGIT
CTLA4
TOX
TOX2
EOMES
scFv-
scFv+
Percent Expressed
Expression Level
K
scFv+ Tcells
SB
LV
CD4
CD8
Percent Expressed
Expression Level
anti-CD19
anti-R110

Figure 4

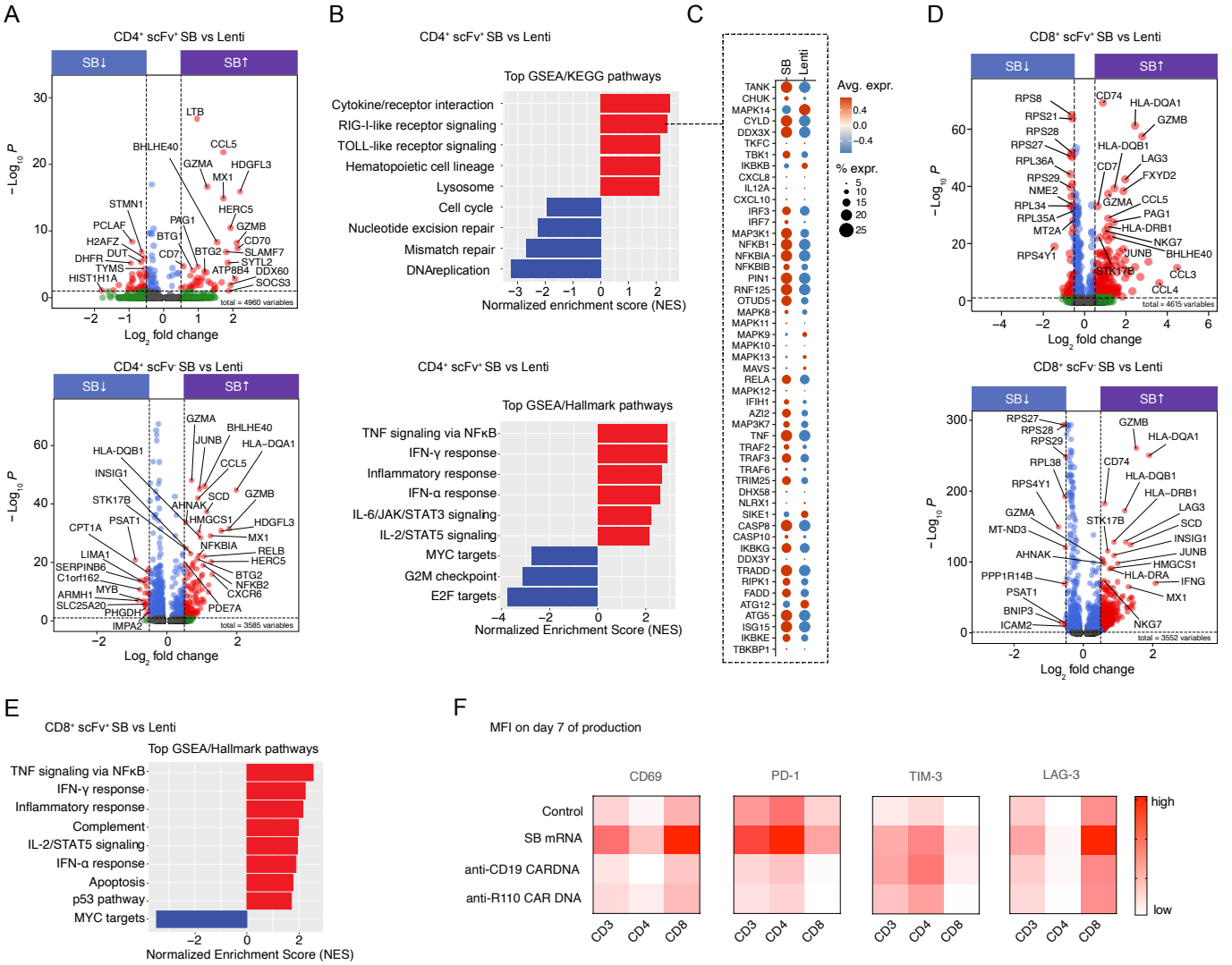
A
CD4+ scFv+ SB vs Lenti
SB↓
SB↑
−Log10 P
Log2 fold change
total = 4960 variables
CD4+ scFv- SB vs Lenti
total = 3585 variables
B
CD4+ scFv+ SB vs Lenti
Top GSEA/KEGG pathways
Cytokine/receptor interaction
RIG-I-like receptor signaling
TOLL-like receptor signaling
Hematopoietic cell lineage
Lysosome
Cell cycle
Nucleotide excision repair
Mismatch repair
DNAreplication
Normalized enrichment score (NES)
CD4+ scFv+ SB vs Lenti
Top GSEA/Hallmark pathways
TNF signaling via NFκB
IFN-γ response
Inflammatory response
IFN-α response
IL-6/JAK/STAT3 signaling
IL-2/STAT5 signaling
MYC targets
G2M checkpoint
E2F targets
Normalized Enrichment Score (NES)
C
SB
Lenti
Avg. expr.
% expr.
D
CD8+ scFv+ SB vs Lenti
total = 4615 variables
CD8+ scFv- SB vs Lenti
total = 3552 variables

E
CD8+ scFv+ SB vs Lenti
Top GSEA/Hallmark pathways
TNF signaling via NFκB
IFN-γ response
Inflammatory response
Complement
IL-2/STAT5 signaling
IFN-α response
Apoptosis
p53 pathway
MYC targets
Normalized Enrichment Score (NES)

F
MFI on day 7 of production
CD69
PD-1
TIM-3
LAG-3
Control
SB mRNA
anti-CD19 CARDNA
anti-R110 CAR DNA
CD3
CD4
CD8
high
low

Figure 5

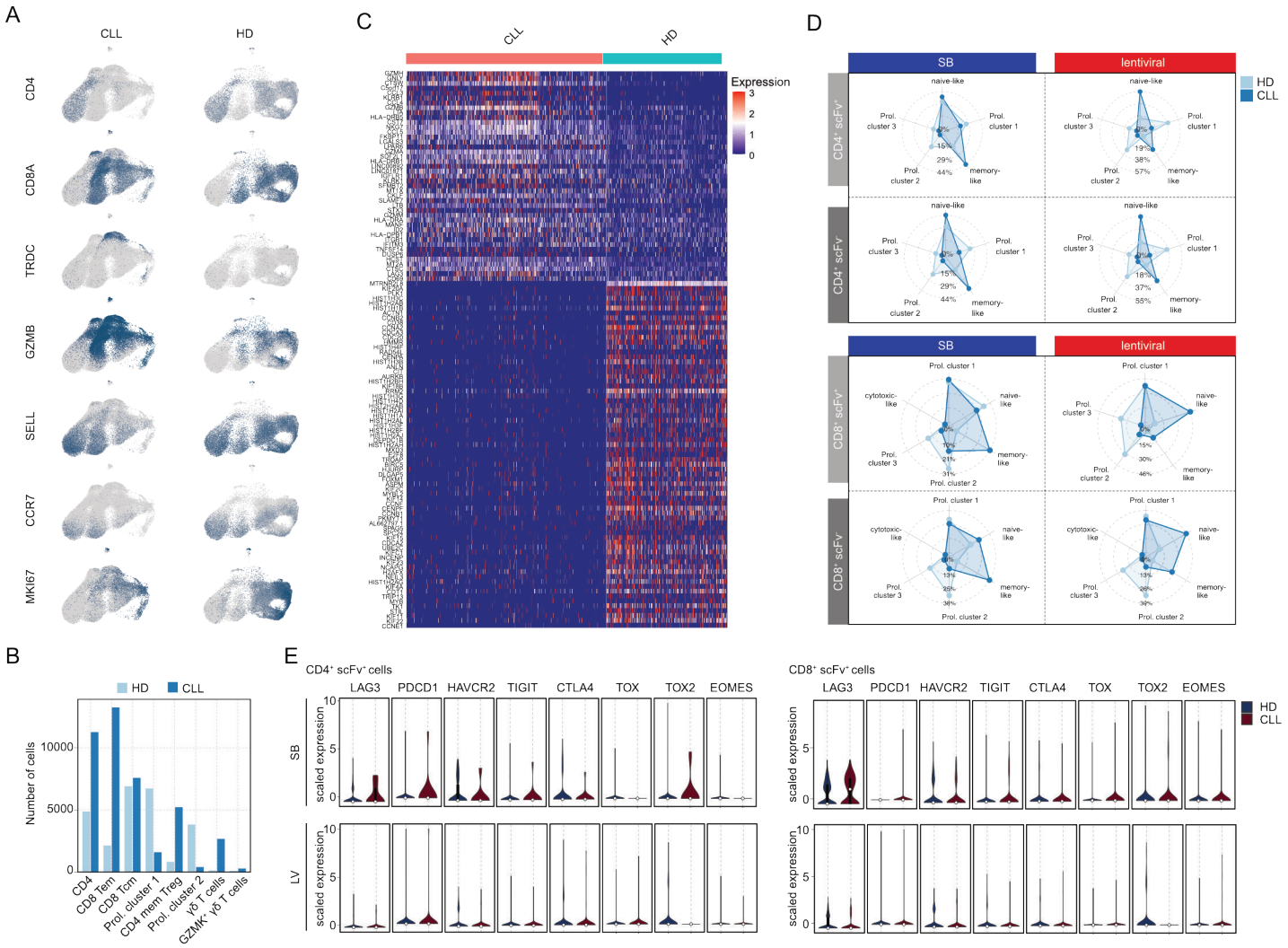
A
CLL
HD
CD4
CD8A
TRDC
GZMB
SELL
CCR7
MKI67
C
CLL
HD
Expression
3
2
1
0
D
SB
lentiviral
HD
CLL
CD4⁺ scFv⁺
CD4⁺ scFv⁻
CD8⁺ scFv⁺
CD8⁺ scFv⁻
naive-like
memory-like
Prol. cluster 1
Prol. cluster 2
Prol. cluster 3
cytotoxic-like
B
HD
CLL
Number of cells
10000
5000
0
CD4
CD8 Tem
CD8 Tcm
Prol. cluster 1
CD4 mem Treg
Prol. cluster 2
γδ T cells
GZMK⁺ γδ T cells
E
CD4⁺ scFv⁺ cells
CD8⁺ scFv⁺ cells
LAG3
PDCD1
HAVCR2
TIGIT
CTLA4
TOX
TOX2
EOMES
SB
LV
scaled expression
10
5
0
HD
CLL

Figure 6

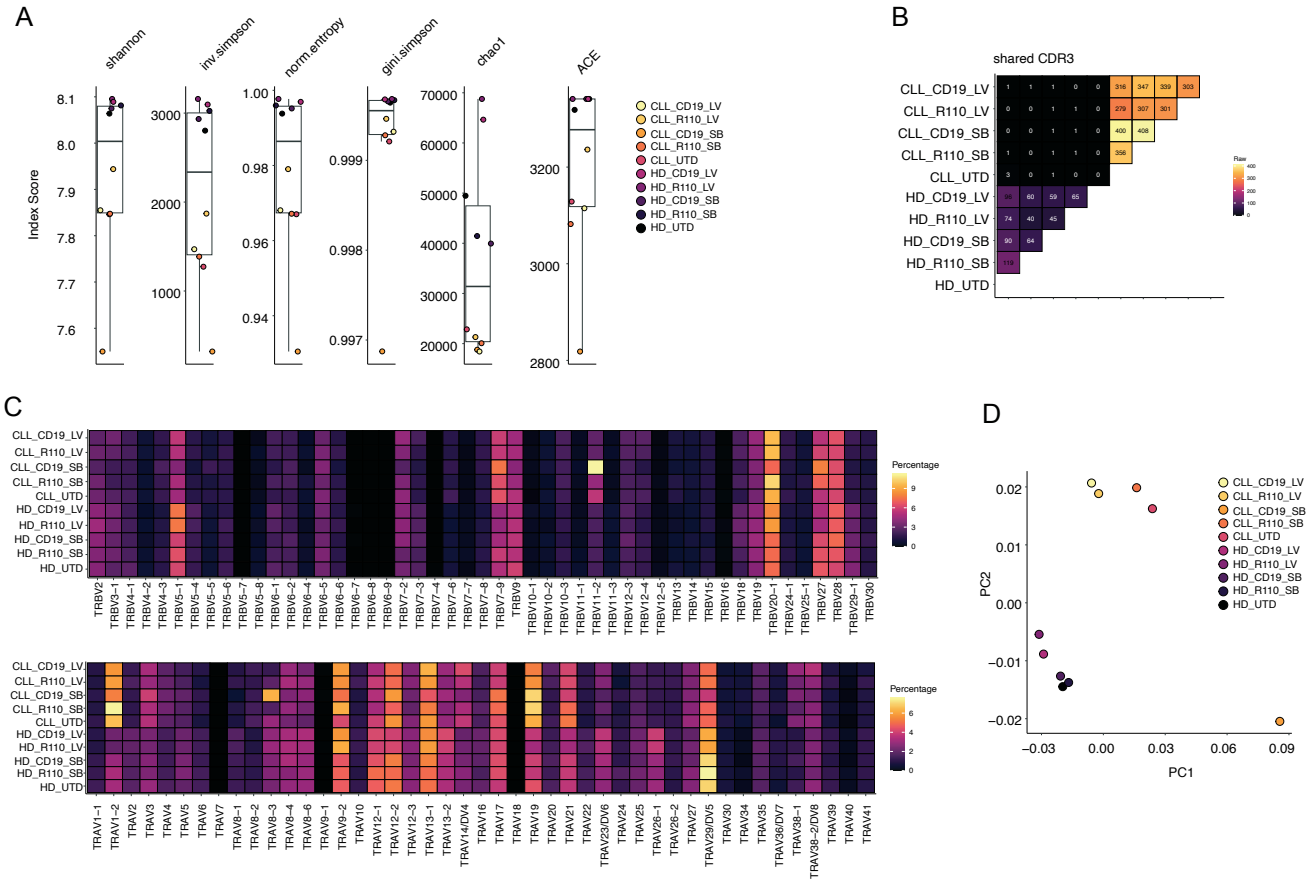
A
shannon
inv.simpson
norm.entropy
gini.simpson
chao1
ACE
Index Score
CLL_CD19_LV
CLL_R110_LV
CLL_CD19_SB
CLL_R110_SB
CLL_UTD
HD_CD19_LV
HD_R110_LV
HD_CD19_SB
HD_R110_SB
HD_UTD
B
shared CDR3
Raw
C
Percentage
D
PC1
PC2

Figure 7

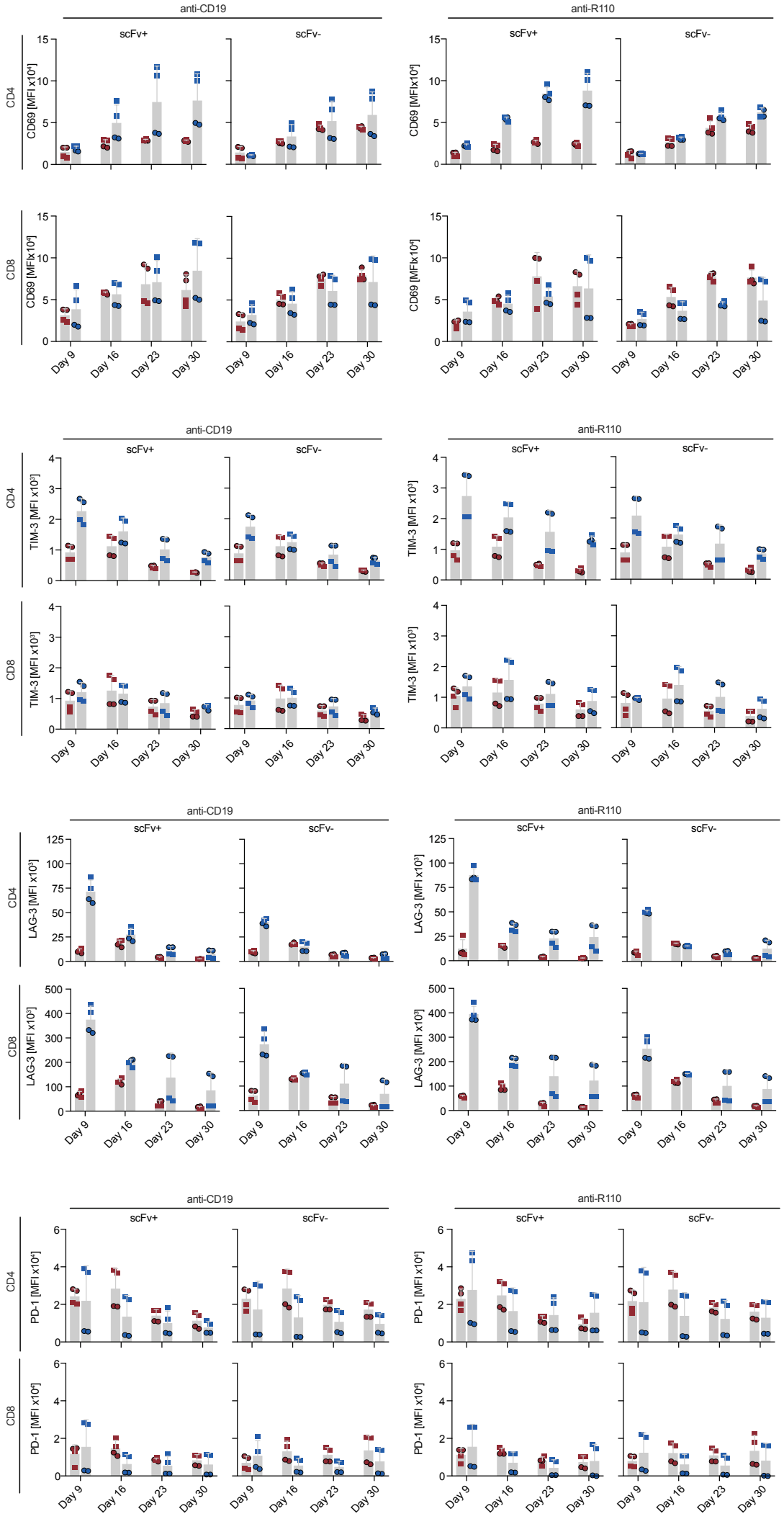
anti-CD19
anti-R110
scFv+
scFv-
CD4
CD8
CD69 [MFI x10⁴]
TIM-3 [MFI x10³]
LAG-3 [MFI x10³]
PD-1 [MFI x10⁴]
Day 9
Day 16
Day 23
Day 30
HD175
CLL456
Lentivirus
HD175
CLL456
Sleeping beauty

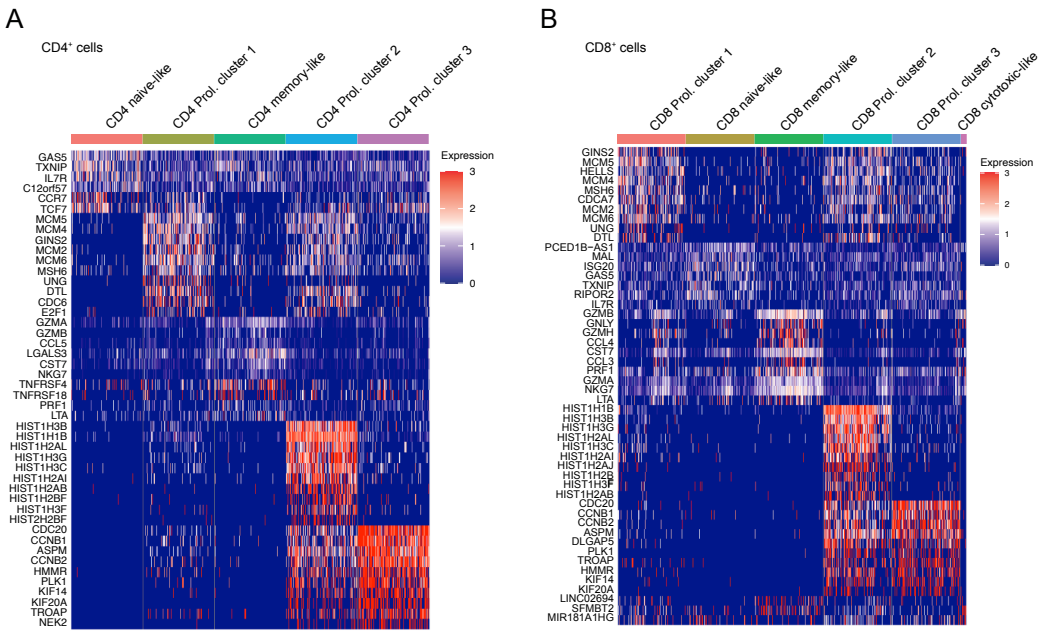

Supplementary Figure 2